Published in final edited form as:
Lab Chip. 2011 November 21; 11(22): 3846–3854. doi:10.1039/c0lc00426j.

Microfluidic waves

Marcel Utz[*,a,c], **Matthew R. Begley**[b], and **Hossein Haj-Hariri**[c]

[a]Center for Microsystems for the Life Sciences, University of Virginia, Charlottesville, VA, 22904, USA

[b]Department of Mechanical Engineering, University of California, Santa Barbara, CA, 93105, USA

[c]Department of Mechanical and Aerospace Engineering, University of Virginia, Charlottesville, VA, 22904, USA

Abstract

The propagation of pressure waves in fluidic channels with elastic covers is discussed in view of applications to flow control in microfluidic devices. A theory is presented which describes pressure waves in the fluid that are coupled to bending waves in the elastic cover. At low frequencies, the lateral bending of the cover dominates over longitudinal bending, leading to propagating, non-dispersive longitudinal pressure waves in the channel. The theory addresses effects due to both the finite viscosity and compressibility of the fluid. The coupled waves propagate without dispersion, as long as the wave length is larger than the channel width. It is shown that in channels of typical microfluidic dimensions, wave velocities in the range of a few 10 m s^{-1} result if the channels are covered by films of a compliant material such as PDMS. The application of this principle to design microfluidic band pass filters based on standing waves is discussed. Characteristic frequencies in the range of a few kHz are readily achieved with quality factors above 30.

1 Introduction

The control of fluid flow and transport in microfluidic devices is key to the implementation of complex biochemical analysis procedures for diagnostic and forensic applications. In many recent device designs, this is accomplished using microfabricated membrane valves which are actuated through external vacuum lines.[1–3] While these valves allow for reliable operation with good domain separation, complex devices require a large number of dedicated pneumatic connections, tethering the chip strongly to substantial off-chip control hardware. Since this is at odds with the goal of high-throughput, expendable, rapid devices that can be deployed at the point of care (diagnostics) or in the field (forensics), alternative approaches to fluid control with potentially more favorable scaling behavior are being explored. This includes diverse strategies such as logic based on bubbles of nonmiscible fluid phases,[4] electrowetting,[5] as well as frequency-specific pumping.[6–8]

The latter approach uses microfabricated deformable features to build microfluidic circuits that behave similar to passive AC electrical circuits consisting of resistors, capacitors, inductors, and diodes. Based on this principle, circuits have been demonstrated recently where the path of liquid transport can be selected simply by changing the operating frequency of a single oscillatory pressure source.[6] So far, these circuits have relied on discrete fluidic capacitors and resistors and were operated at relatively low frequencies up to

*mu3q@virginia.edu.

a few Hz. In this frequency range, the inductance provided by the inertia of the fluid plays only a minor role, and it is very difficult to achieve mechanical resonance, which would allow to construct filters with narrow bandwidths.

As shown in the remainder of this paper, devices with much more narrow bandwidth are possible on the basis of the propagation of pressure waves in microfludic channels with deformable capping layers. Linear fluidic channels provide a certain amount of resistance (due to viscous losses), capacitance (due to the elasticity of the material covering the channel), and inductance (due to the inertia of the fluid transported in the channel). In analogy to a coaxial cable, which can be seen as the combination of a distributed (electrical) capacitance and inductance, microfluidic channels must therefore be expected to be able to act as waveguides. Indeed, even in a completely rigid channel, pressure waves can propagate due to the finite compressibility of the fluid. However, in the case of aqueous fluids, the frequencies corresponding to wavelengths in the range between 1 mm and 10 mm are of the order of 10^7 Hz, much too high for microfluidic actuation.

The present contribution lays out the theory of pressure waves in microfluidic channels with elastic capping layers. Consider a microfluidic channel of depth h in an ideally rigid matrix, as shown in Fig. 1. The cover is made of an elastic solid, with Young's modulus E, of thickness d. The width b of the channel is assumed to be much larger than the depth. As will be shown in the following, waves in the desired range to build wavelength-based filters (1~10 mm) and frequencies in the range of kHz can easily be obtained in microfluidic channels if the cover is sufficiently compliant.

The problem under study here is somewhat similar to the propagation of pressure waves in elastic tubes, which has been studied extensively, due to the relevance to flow in blood vessels[9–17] (for a brief and lucid review, see ref. 18). However, spite of the obvious similarities, there are significant differences between the microfluidic and vascular problem, which warrant a separate treatment: Obviously, microfluidic channels are cylindrically symmetrical. In addition, the finite compressibility of the fluid must be taken into consideration, at least for stiffer cover materials. Finally, the longitudinal elasticity of blood vessels is an essential feature, whereas microfluidic channels be regarded as stiff in this direction.

2 Theory

2.1 Channel cover bending

The channel cover can be regarded as a rectangular plate, clamped at $y = \pm b/2$. In the following, we will assume the pressure in the fluid to be a function of x only. Furthermore, we will assume it to vary slowly over distances comparable to the channel width. For the deflection of the cover, we can therefore write

$$\zeta(x,y) = \xi(x)\, f(y), \tag{1}$$

where $f(y) = 1 - 8y^2/b^2 + 16y^4/b^4$ is the transverse shape function, and $\xi(x)$ denotes the deflection of the center line. In the case of a constant pressure $p(x)$, this corresponds to the classical plate solution (with ξ = const.), and remains a very good approximation as long as the wavelength of $\xi(x)$ is large compared to the channel width. The deflection function ζ satisfies the biharmonic equation[19]

$$D\Delta^2\zeta - p(x) = 0, \tag{2}$$

where $D = Ed^3/12(1 - \nu^2)$ is the flexural stiffness of the cover. Inserting (1) into (2) and integrating over the y coordinate yields

$$p = \frac{384D}{b^4}\xi + \frac{8D}{15}\frac{\partial^4 \xi}{\partial x^4} \tag{3}$$

In the case of a harmonic deflection $\xi(x) = \tilde{\xi} \exp ikx$ with wave number k, this becomes

$$\tilde{p} = \frac{384D}{b^4}\tilde{\xi} + \frac{8D}{15}k^4\tilde{\xi}, \tag{4}$$

where $\tilde{p}$ and $\tilde{\xi}$ are the complex amplitudes of the pressure and the deflection, respectively. The second term on the right hand side scales with k^4, and remains negligible as long as

$$720 \gg (kb)^4. \tag{5}$$

Therefore, longitudinal pressure waves in the channel are governed purely by the transverse stiffness, and not by longitudinal bending of the cover, as long as the wave length $\lambda = 2\pi/k$ satisfies

$$\lambda \gg \lambda_{\min} = \frac{2\pi b}{\sqrt[4]{720}} \approx 1.22\, b. \tag{6}$$

In practice, the ratio of channel width to cover thickness b/d ranges from about 1 to 10. In this range, the ideal plate solution discussed above is a reasonable assumption, but tends to underestimate the stiffness. In the limit $b/d < 1$, the behavior is closer to that of an infinite half-space. Seker *et al.* have given a universal interpolation function for the flexural stiffness that matches finite element results across all ratios b/d with errors of less than 6% for small deflections:[20]

$$p(x) = \frac{E}{(1 - \nu^2)\, b\, F_i(b/d)}\xi(x), \tag{7}$$

with the interpolation function

$$F_i\left(\frac{b}{d}\right) = 1 + \frac{1}{4}\left(\frac{b}{d}\right)^{\frac{7}{4}} + \frac{1}{32}\left(\frac{b}{d}\right)^3. \tag{8}$$

This interpolation can be used in the present context by setting the flexural stiffness

$$D = \frac{E\, b^3}{384\,(1 - \nu^2)\, F_i(b/d)}. \tag{9}$$

2.2 Wave equation

In order to derive a coupled wave propagation equation for pressure waves in the channel, we assume the flow profile to be homogeneous at all times over the width of the channel, in keeping with the assumption $b \gg h$. The goal is to capture the following physical details of

the process: (i) the coupled bending of the capping layer and fluid motion, (ii) the finite viscosity of the fluid, and (iii) the influence of the inertia of the capping layer.

In the following, x is the direction of the channel axis, z is the vertical, normal to the chip plane, and y the lateral direction. The bottom of the channel corresponds to $z = 0$, and the top to $z = h + \xi$, where h is the channel height at vanishing pressure, and ξ the transient vertical deflection. We will denote the x component of the velocity field as $u = u(x, z, t)$.

In the limit of small displacements ($\xi \ll h$), the vertical velocity components can be neglected from the momentum balance and the continuity equations. The mass of fluid contained in a slice of the channel of thickness dx can change due to (i) changing channel deflection dξ, (ii) fluid compression due to pressure change dp, and (iii) differential flow velocity into and out of the slice dx. Mass conservation therefore yields the continuity equation

$$\frac{8}{15}\frac{\partial \xi}{\partial t}+h\kappa\frac{\partial p}{\partial t}+\frac{\partial}{\partial x}\int_0^h u\,\mathrm{d}z=0, \tag{10}$$

where κ is the compressibility of the fluid. The factor 8/15 in the first term is due to the integral of the shape function $f(y)$. Neglecting vertical velocity components, momentum conservation in the x direction for a fluid volume element of dimensions dx dz gives to first order (for small velocities)

$$\rho\frac{\partial u}{\partial t}=-\frac{\partial p}{\partial x}+\eta\frac{\partial^2 u}{\partial z^2}, \tag{11}$$

where ρ and η are the density and dynamic viscosity of the fluid, respectively, and $p(x, t)$ is the pressure, assumed to be uniform over the vertical (z) dimension.

No-slip boundary conditions are applied at $z = 0$ and $z = h$:

$$u(x,0,t)=0 \text{ and } u(x,h,t)=0. \tag{12}$$

In the limit of low frequencies, the velocity profile through the depth of the channel assumes a parabolic shape

$$u(x,z,t)=q(x,t)\frac{6z}{h^2 b}\left(1-\frac{z}{h}\right). \tag{13}$$

$q(x,t)$ is the volumetric flow rate through the channel, since

$$\int_0^h u\,\mathrm{d}z=\frac{q(x,t)}{b}. \tag{14}$$

However, at higher frequency, it is well known that the flow profile deviates from this shape,[8,12] depending on the kinematic viscosity of the fluid and the height of the channel. This is related to the start-up time required for a parabolic profile to establish itself upon sudden switching on of a pressure gradient. As detailed in Appendix A, the shape of the flow profile is controlled by the dimensionless frequency[8,12]

$$\alpha=\frac{\rho\omega h^2}{\eta}; \tag{15}$$

for values of α below about 20, a parabolic flow profile is obtained, whereas for $\alpha > 20$ the profile transitions to plug flow. In the latter case, the majority of the viscous loss is confined to a narrow region close to the boundaries.

Once the shape of the flow profile is known, the momentum balance equation can be integrated over the z coordinate to give (*cf.* Appendix A)

$$\frac{\rho}{bh}\frac{\partial q}{\partial t}+\frac{12\eta\sqrt{1+\alpha/72}}{bh^3}q=-\frac{\partial p}{\partial x}. \tag{16}$$

In the following, we will take into account the dependence of the viscous dissipation term on α by introducing an apparent viscosity

$$\overline{\eta}=\eta\sqrt{1+\alpha/72}. \tag{17}$$

Combining (10) with (14) gives

$$\frac{8}{15}\frac{\partial \xi}{\partial t}+h\kappa\frac{\partial p}{\partial t}+\frac{1}{b}\frac{\partial q}{\partial x}=0. \tag{18}$$

By combining (16) and (18), and eliminating the flow rate q, one obtains the wave equation

$$\frac{8}{15}\frac{\partial^2 \xi}{\partial t^2}+h\kappa\frac{\partial^2 p}{\partial t^2}+\frac{12\overline{\eta}}{\rho h^2}\left(\frac{8}{15}\frac{\partial \xi}{\partial t}+h\kappa\frac{\partial p}{\partial t}\right)=\frac{h}{\rho}\frac{\partial^2 p}{\partial x^2}. \tag{19}$$

In the case of a rigid channel ($\xi = 0$), this reduces to

$$\frac{\partial^2 p}{\partial t^2}+\frac{12\overline{\eta}}{\rho h^2}\frac{\partial p}{\partial t}=\frac{1}{\kappa p}\frac{\partial^2 p}{\partial x^2}, \tag{20}$$

which is simply the governing equation for sound propagation in the fluid. Conversely, in the case of an incompressible fluid, we have $\kappa = 0$, and (19) becomes

$$\frac{\partial^2 \xi}{\partial t^2}+\frac{12\overline{\eta}}{\rho h^2}\frac{\partial \xi}{\partial t}=\frac{15h}{8p}\frac{\partial^2 p}{\partial x^2}. \tag{21}$$

As will be seen in the following, it is not necessary to make either of these simplifying assumptions to derive a dispersion relation, *i.e.*, an analytical expression can be found for the completely general case described by (19). However, the expression is very lengthy, and it will be shown that for practical geometries, there is a range of wavelengths where the fluid can be treated as incompressible to a good approximation.

2.3 Dispersion relation

The main motivation for the present work is the design of microfluidic networks with frequency-specific responses due to the formation of standing waves in fluidic channels of appropriately chosen dimensions. In order to accomplish this, it is necessary to derive the relationship between frequency and wavelength or wave vector, commonly referred to as the dispersion relation.

The relationship derived above between the deflection and the pressure, (3), can be used to obtain an equation of motion for the deflection ξ. In the case of a time-dependent pressure $p(x, t)$, (3) must be completed with an inertial term:

$$p(x,t)=\frac{384D}{b^4}\xi+\frac{8D}{15}\frac{\partial^4\xi}{\partial x^4}+\frac{8}{15}d\rho_c\frac{\partial^2\xi}{\partial t^2}, \tag{22}$$

where ρ_c is the density of the cover material. With (19), and assuming a harmonic deflection

$$\xi(x,t)=\xi_0 e^{i(kx-\omega t)} \tag{23}$$

one obtains the quartic dispersion relation

$$\sum_{j=0}^{4} a_j(k)\quad \omega^j=0, \tag{24}$$

with the coefficients

$$a_0=\frac{384Dhk^2}{b^4\rho}+\frac{8Dhk^6}{15\rho} \tag{25}$$

$$a_1=-i\frac{\overline{\eta}}{\rho}\left(\frac{32\left(1+Dhk^4\right)}{5h^2}+\frac{4608D\kappa}{b^4h}\right) \tag{26}$$

$$a_2=-\frac{8}{15}\left(1+\frac{dh\rho_c}{\rho}k^2\right)-Dh\kappa\left(\frac{8k^4}{15}+\frac{384}{b^4}\right) \tag{27}$$

$$a_3=i\frac{32d\overline{\eta}\kappa\rho_c}{5h\rho} \tag{28}$$

$$a_4=\frac{8}{15}dh\kappa\rho_c \tag{29}$$

For any given wave number $k = 2\pi/\lambda$, the dispersion relation therefore is a polynomial of order 4 in the frequency ω, with coefficients that depend on k in a non-linear fashion. This equation can be solved for ω analytically, even though the expressions are very unwieldy.

The physical meaning of the solutions is more easily grasped by converting the dispersion relation into a dimensionless form. To this effect, the wave vector and frequency are normalized using the channel width b and the speed of sound in the fluid $1/\sqrt{\kappa\rho}$ as

$$K=k\,b \quad \text{and} \quad \Omega=\omega\,b\sqrt{\kappa\rho}. \tag{30}$$

In the inviscid case ($\overline{\eta}=0$), the dispersion relation then becomes

$$(K-\Omega)(K+\Omega)\left(1+K^4/720-\Omega^2/B^2\right)=A\Omega^2, \tag{31}$$

with the two dimensionless constants

$$A=\frac{b^4}{720D\kappa} \quad \text{and} \quad B^2=\frac{720D\kappa\rho}{b^2 d\rho_c}. \tag{32}$$

The four branches of solutions $\Omega_l(K)$, $l = 1\ldots4$ are pair-wise equivalent to each other, representing waves traveling in opposite directions. This leaves two classes of solutions, shown in Fig. 2. The solid lines represent the case where $A = 0$ and $B = 10$. A plays the role of a coupling constant. In the case of vanishing A, the equation is separable. The red line is then essentially the dispersion relation for sound waves in the fluid. Due to the normalization, it passes through the point $(K, \Omega) = (1, 1)$. In the doubly logarithmic plot, its slope is unity, indicating that the waves propagate without dispersion. By contrast, the blue solid line represents waves in the cover layer. At large values of K, corresponding to wavelengths shorter than the width of the channel, they propagate as bending waves, governed by the longitudinal bending stiffness of the cover. The slope is 2 in this case, indicating the dispersive nature of these waves. For wavelengths above the channel width ($K < 1$), the frequency is independent of the wave vector, converging to a constant in the limit $K \rightarrow 0$. In this regime, the normalized group velocity $C_g = \partial\Omega/\partial K$ vanishes, indicating that local perturbations in the amplitude of these wave modes do not propagate along the channel. The limiting frequency is given by

$$\Omega_{\text{opt}}=B\sqrt{1+A}. \tag{33}$$

The dimensionless parameter B therefore represents the eigenfrequency of the cover layer, expressed in units of $b\sqrt{\kappa\rho}$, and essentially controls the vertical position of the blue branch of the dispersion relation.

Increasing A leads to coupling of the wave modes, as shown by the dashed lines in Fig. 2. At small K, this reduces the frequencies in the red branch and increases the ones in the blue branch, both by a factor of $\sqrt{1+A}$. In analogy to the physics of lattice vibrations in crystals, we refer to the two branches of the dispersion relation as the “optical” (blue) and “acoustic” (red) branches, respectively.

In the present context, it is the low-K region of the acoustic branch that is of interest. The dimensionless coupling parameter A is given by the ratio of the compliance of the cover, b^4/D, to that of the compressible fluid underneath, $h\kappa$. Large values of A lead to a substantial reduction in the phase velocity of pressure waves in the fluid, which is given by

$$c_p=\frac{1}{\sqrt{\kappa\rho}}\frac{\Omega}{K}=\frac{1}{\sqrt{1+A}\sqrt{\kappa\rho}}. \tag{34}$$

Fig. 3a shows a map of the dimensionless parameters A and B. The area where $A > 1$ represents the case of strong coupling, where the propagation of pressure waves is significantly slowed by the compliance of the cover. $B > 1$ corresponds to a stiff cover, *i.e.*, the eigen frequency of the cover by itself is large compared to the frequency of transverse standing sound waves in the channel.

The solid lines in Fig. 3a represent water-filled microfluidic channels of typical geometry, channel depth $h = 0.2$ mm, covered by three different types of materials: (i) a layer of glass of 100 μm thickness (red line), (ii) a layer of 20 μm Poly(styrene), a glassy polymer(orange

line), and (iii) a layer of poly(dimethyl siloxane) (PDMS) of 280 μm thickness. The lines have been obtained by varying the channel width from 0.2 to 1.5 mm, as indicated in the figure. It is obvious that for these geometries, the behavior of the glass and polymer covers is quite different. While the glass covered channels fall into the stiff and weakly coupled regime, both the PDMS and Polystyrene covers represent soft, strongly coupled systems.

The resulting phase velocities are shown in Fig. 3b. Pressure waves propagate at substantially reduced velocities compared to the speed of sound in water (~1450 m s^{-1}) in all cases, except for the narrowest glass-covered channels. This velocity reduction amounts to several orders of magnitude when softer, polymeric cover materials are used. Indeed, phase velocities in the range of tens of ms^{-1} are readily accessible with elastomeric covers (represented in Fig. 3 by PDMS). This amounts to a combination of kHz frequencies and wavelengths in the range of a few cm. As will be discussed in detail below, this is ideal for the construction of frequency-selective fluidic networks based on standing wave modes.

2.4 Microfluidic waves

In the following, we will focus our attention on acoustic waves under strong coupling ($A \gg 1$), and limit the discussion to long wavelengths ($K = kb < 1$). As shown in the previous section, this is a good approximation to describe pressure waves propagating in a microfluidic channel with a compliant cover. In this case, the phase velocity becomes independent of the compressibility of the fluid, and is governed solely by the bending stiffness of the cover and the fluid density:

$$c_p \approx \sqrt{\frac{720Dh}{b^4\rho}}. \tag{35}$$

In order to capture the damping behavior of microfluidic waves, the finite viscosity of the fluid must be taken into account. Neglecting terms of higher order in k and setting $\kappa \to 0$, the dispersion relation (24) to (29) becomes:

$$\omega^2 + 12i\gamma\sqrt{1+\alpha/72}\,\omega = c_p^2 k^2, \tag{36}$$

which depends on only two parameters: the phase velocity c_p given by (35) and the damping parameter $\gamma = \eta/h^2\rho$. This relation can be rewritten in normalized form in terms of the non-dimensional frequency $\alpha = \omega/\gamma$ and the non-dimensional wave vector $\bar{k} = k_{cp}/\gamma$ as

$$\alpha^2 + 12i\alpha\sqrt{1+\alpha/72} = \bar{k}^2, \tag{37}$$

with the general solution

$$\bar{k} = \pm\alpha\sqrt{1+\frac{12i}{\alpha}\sqrt{1+\alpha/72}}. \tag{38}$$

The real and imaginary part of this solution are plotted in Fig. 4. For a given, real frequency, these solutions represent propagating waves with a wavelength given by the real part of $2\pi/\bar{k}$, and a decay length (distance from the source over which the wave amplitude decreases by a factor of e) given by the imaginary part. As can be seen in the figure, these two lengths coincide for frequencies $\alpha < 1$, indicating that the waves are overdamped in this regime. By contrast, true propagating waves exist at higher frequencies. The ratio between

the real and imaginary part of $\bar{k}$ can be viewed as a quality factor, which is also plotted in Fig. 4.

2.5 Damping

As discussed earlier, the apparent viscosity $\bar{\eta}$ depends weakly on the frequency due to transition from Poiseuille- to plug flow at higher frequencies. While this only has a negligible effect on the oscillatory behavior, damping is directly affected by the increased viscosity. Damping can be manifested in the propagation of waves in time or in space. The first case concerns the decay time of a harmonic wave mode (with equal amplitude everywhere). In this case, the wave vector $\bar{k}$ is real, and the frequency has a real (oscillatory) and imaginary (damping) part. More relevant in view of the present applications is the opposite case, where the frequency is real, and $\bar{k}$ is a complex quantity, as shown in Fig. 4. This represents the free propagation of waves away from a source oscillating at a given frequency. In this case, the oscillations persist in time, as long as the excitation is maintained, but decay with increasing distance from the source.

Expanding the outer square root in (38) to first order, one obtains for the specific insertion power loss (in dB per unit length)

$$\frac{20}{\ln 10}\mathrm{Im}\,[k] \approx \frac{20}{\ln 10}\frac{6\gamma}{c_p}\sqrt{1+\alpha/72}. \tag{39}$$

The insertion loss is proportional to the damping constant, and inversely proportional to the wave velocity. The insertion loss for the same materials and geometries considered above is plotted in Fig. 5a, assuming a typical frequency of 5kHz. Obviously, due to the high phase velocity, the insertion loss is very small for a stiff glass cover. In the case of the much more compliant PDMS and PS covers, the losses amount to a few dB cm^{-1}. Somewhat counterintuitively, the loss *increases* with the channel width, due to the decreasing phase velocity in wider channels.

2.6 Wave transport

The transmission of waves through fluidic channels is governed by the fluidic impedance, given by the ratio

$$Z_0 = \frac{p\,(x,t)}{q\,(x,t)}. \tag{40}$$

Expressing both p and q in terms of the deflection $\xi(x, t)$, the impedance Z_0 can be found as a function of the channel parameters. While p is given in terms of ξ by eqn (22), the flow rate q is found by integrating (18) over x. To the present approximations, one finds

$$Z_0 = \frac{720D}{b^5}\frac{k}{\omega} = \frac{720D}{b^5 c_p} = 12\sqrt{\frac{5D\rho}{b^6 h}}. \tag{41}$$

Fig. 5b shows the wave impedance as a function of channel width for the three cover materials discussed previously.

3 Applications in microfluidics

3.1 General requirements

The main motivation to develop the theory of microfluidic waves was their potential use for flow control in microfluidic devices. Such devices can be designed following either a time-domain paradigm, in which distinct pathways in the device are designed to lead to specified transmission times for pressure pulses, or in a frequency-domain paradigm, where channels are designed to selectively transmit harmonic signals of particular frequencies. In either case, a number of requirements must be satisfied.

Ultimately, the waves have to interact with other fluidic circuit elements, such as valves, diodes, resistors, and capacitors. These elements have switching times in the millisecond range at best. Correspondingly, the microfluidic wave frequencies must not substantially exceed 10 kHz. An obvious requirement is therefore that propagating waves must exist in this frequency range, and they must not be excessively damped. In order to be able to design time-domain circuits that depend on the transmission times of pulses, it is also important that the waves be nondispersive. The same property also ensures that networks can be universally matched, *i.e.*, the wave impedance does not depend on frequency. As shown above, microfluidic waves in the strong coupling regime do satisfy this requirement.

Practical microfluidic devices are tens of mm in size. Timed or frequency-specific networks must conform to these dimensions, which dictates the upper limit of useful wave lengths. The lower limit is given by the channel widths, which are typically tens to hundreds of μm. To be compatible with the millisecond switching times of microfluidic valves and diodes, this sets an upper bound for the wave velocity in the range of about $c_{\max} \approx 10\ \text{mm} \times 10\ \text{kHz} = 100\ \text{m s}^{-1}$. Waves propagating substantially faster than this value would lead to either impractical channel lengths or unmanageably high frequencies. Fig. 3b shows that the PDMS cover satisfies this requirement over a wide range of channel widths, whereas the Poly(styrene) thin film does so only for relatively wide channels ($b > 0.5\text{mm}$). By contrast, the glass cover gives a value above 300 m s^{-1} over the entire range of channel widths shown in the figure. This also illustrates why pure sound waves in a rigid channel would be of no use in the present context.

In combining microfluidic wave guide channels with other switching elements, such as membrane valves and diodes, impedance matching is an important consideration. As is well known, traveling waves are reflected, unless the channel guiding the wave is connected to a resistance equal (or close) to its characteristic impedance. In order to successfully integrate microfluidic waves with conventional microfluidics, the characteristic impedances of the wave guides must therefore be in a similar range to the resistances of typical switching elements.

Microfluidic devices typically operate with flow rates in the range of nanolitres up to microlitres per second, and at pressures in the kPa range. These values determine the design of capacitors, valves, and other elements of microfluidic networks. In order to be integrated into this kind of environment, fluidic wave guides must exhibit wave impedances that are similar to typical resistances. As can be seen in Fig. 5b, the PDMS cover gives impedances of less than 1 kPa s $(\mu\text{l})^{-1}$ over the entire range of channel widths, as does the PS cover for $b > 0.5$ mm. By contrast, the stiff glass cover yields very high impedances. It should also be noted that the wave impedance scales with b^{-3}. This strong dependence is an advantage, since it facilitates the design of frequency-specific fluidic networks based on standing waves, as discussed in the next section.

3.2 Application example: Fluidic filters

The propagation of microfluidic waves in a network of channels combined with other fluidic circuit elements can be seen as a classic scattering problem, and can be treated in a way similar to electrical network theory.[21] The two traveling wave modes (forward and backward propagation) are represented by the complex amplitudes $\alpha_j^{\alpha,\beta}$, which are defined such that their absolute square represents the power transported by the wave at the midpoint of the j-th channel in the network:

$$a_j^{\alpha,\beta}=q_j^{\alpha,\beta}/\sqrt{Z_j}=p_j^{\alpha,\beta}\sqrt{Z_j}. \tag{42}$$

Incoming waves at a junction are scattered into all channels connected to it. The amplitudes of the scattered waves are determined by the requirement that the power carried by the incoming and outgoing waves be equal, and that the sum of all flow rates vanish at the junction.

In the simplest case of a step change in the channel width, shown in Fig. 6, this leads to the reflection ratio

$$r=\frac{Z_j-Z_m}{Z_j+Z_m}, \tag{43}$$

where Z_j is the impedance of channel segment j, and Z_m is the impedance of the channel segment after the step change. The coupling between the two modes a_j^{α} and a_j^{β} is then given by

$$a_j^{\beta}=a_j^{\alpha}\, r\, e^{ik_j(\omega)l_j}, \tag{44}$$

where $k_j(\omega)$ is the wave number in wave guide j, and l_j its length, and it is assumed that the α mode is traveling into the junction, whereas β is traveling away from it. In a similar way, the transmitted wave amplitude is

$$a_m^{\alpha}=a_j^{\alpha}e^{\frac{i}{2}(k_jl_j+k_ml_m)}\,(1-r)\,. \tag{45}$$

The simple fluidic circuit shown in Fig. 6 has been modeled in this way. The dependence of the wave velocity and the wave impedance on the channel dimensions and the properties of the fluid and the elastic cover are given by eqn (35) and (41). Viscous dissipation is taken into account through the imaginary part of the wave vector (39), which causes waves excited at one end of a channel to decrease exponentially in amplitude with distance from the source.

Fig. 6 shows the transmission characteristic for a fluidic channel filter connected in series. The material parameters are those for water and PDMS, with a cover thickness of 280 μm and channel dimensions as indicated in the figure. The circuit behaves as a narrow band pass at a fundamental frequency close to 3 kHz, and all integer harmonics. The width of the peaks is 75 Hz at the −3 dB point (half height) and 400 Hz at the −10 dB point, corresponding to a quality factor around 40.

4 Conclusions

A one-dimensional theory of wave propagation in fluidic channels with elastic covers has been developed, including effects of the finite viscosity and compressibility of the fluid. For channel dimensions typical of microfluidic devices, it was found that nondispersive waves with velocities in the range of tens of meters exist if the channel cover is made of a highly compliant material, such as PDMS. It has been shown theoretically that it is possible to build fluidic filter circuits with Q factors of more than 30 using this principle.

Acknowledgments

It is a pleasure to acknowledge helpful discussions with Prof. James Landers and Prof. Michael Reed. This work has been supported by the National Science Foundation under grant number DMR-0647790 and CHE-0809795, as well as by the National Institute of Health under grant number 1R01-EB011591-01.

A Oscillatory flow profiles in shallow channels

As has been shown by a number of authors, the flow profile in a confined channel under oscillatory pressure is only parabolic in the limit of low frequencies.[8,12] This leads to a weak frequency dependence of the flow resistance, which has been taken into account in the foregoing theory of fluidic waves. In the following, the frequency-dependent resistance is derived for a rectangular channel of width b and depth h, under the assumption of $b \gg h$.

Momentum balance in the axial (x) direction on a volume element of height dz, width b, and length dx requires that

$$\rho \frac{\partial u(x,z,t)}{\partial t} = -\frac{\partial p}{\partial x} - \eta \frac{\partial^2 u(x,z,t)}{\partial z^2}, \tag{46}$$

where $u(x, z, t)$ is the x-component of the velocity field in the fluid.

We assume an oscillatory pressure input, with an amplitude that depends on axial position in general:

$$\frac{\partial p}{\partial x} = D_p(x) \exp i\omega t, \tag{47}$$

where D_p denotes the local pressure amplitude. Similarly, the resulting flow field can be separated into a local flow rate amplitude $q(x)$, a velocity profile function $v(z/h)$, and a harmonic time dependence:

$$u(x,z,t) = q(x)\ v(z/h) \exp i\omega t. \tag{48}$$

Note that both the velocity profile function and the flow rate amplitude are complex in general, expressing magnitude as well as phase of the local velocity field with respect to the oscillations of the pressure gradient.

Introducing this into the momentum balance equation, one obtains a differential equation for the velocity profile function $v(s)$, with the substitution $z/h \rightarrow s$:

$$i\omega\rho v(s) + \frac{\eta}{h^2} \frac{\mathrm{d}^2 v(s)}{\mathrm{d}s^2} = -bh \frac{D_p(x)}{q(x)} \tag{49}$$

The quantity $R_0 = D_p(x)/q(x)$ on the right hand side is the (complex) specific flow resistance of the channel. For a given (but yet to be determined in terms of the channel geometry and fluid properties) value of R_0, the above equation is an inhomogeneous linear differential equation with constant coefficients. It is advantageous to choose the coordinate system in a symmetrical fashion such that the bottom and top of the channel are represented by values of $s = \pm 1/2$. Non-slip boundary conditions therefore require $v(\pm 1/2) = 0$. The velocity profile function then is

$$v(s) = R_0 \frac{bh^3}{\eta}\left(\frac{\cosh\sqrt{-i\alpha s}}{\cosh\sqrt{-i\alpha/2}} - 1\right), \tag{50}$$

with the Womersley parameter

$$\alpha = \frac{\omega\rho h^2}{\eta}, \tag{51}$$

which compares the time scale for establishing a stationary, parabolic flow profile upon flow startup to the period of oscillation. In the limit $\alpha \to 0$, the parabolic flow profile is recovered:

$$\lim_{\alpha\to 0} v(s) = \frac{R_0 bh^3}{8\eta}\left(4s^2 - 1\right). \tag{52}$$

Flow profiles for different values of α are shown in Fig. 8. Upon increasing α, the profile transitions from a parabolic shape to a plug flow.

The flow resistance R_0 is obtained from the requirement that the velocity profile function $v(s)$ be normalized:

$$\int_{-\frac{1}{2}}^{\frac{1}{2}} v(s)\, ds = 1. \tag{53}$$

One finds

$$R_0 = -\frac{\eta}{bh^3}\frac{i\alpha^{\frac{3}{2}}}{\sqrt{\alpha} + 2\sqrt{i}\tanh\left(i\sqrt{i\alpha}/2\right)}. \tag{54}$$

To an excellent approximation over all ranges of α, this expression can be replaced with the much simpler

$$R_0 \approx \frac{\eta}{bh^3}\left(\sqrt{144 + 2\alpha} - i\alpha\right). \tag{55}$$

Normalized values of the imaginary and real parts of these expressions are shown in Fig. 7. The real (inertial) part of the flow resistance increases linearly with α over the entire range. At low $\alpha < 20$, the imaginary part (representing viscous dissipation) remains constant, whereas it increases proportionally to $\sqrt{\alpha}$ at high frequencies.

The fluidic resistance can be written as $R_0 = R - i\omega L$, where R is inductance is the specific resistance, and L is the specific inductance (sometimes also referred to as "inertance") due to inertia. Together with (51), we obtain

$$R=\frac{n}{bh^3}\sqrt{144+2\alpha} \quad L=\frac{\rho}{bh}. \tag{56}$$

These quantities can be used to formulate a momentum balance in terms of the flow rate:

$$L\frac{\partial q}{\partial t}+Rq=-\frac{\partial p}{\partial x} \tag{57}$$

or, explicitly

$$\frac{\rho}{bh}\frac{\partial q}{\partial t}+\frac{\eta}{bh^3}\sqrt{144+2\alpha} \quad q=-\frac{\partial p}{\partial x}, \tag{58}$$

which is identical to eqn (16).

The ratio of the imaginary and real parts of R_0 is the quality factor of a microfluidic channel. In the case of a tuned system (by coupling to a capacitive element), a quality factor larger than unity indicates an underdamped system, in which resonance leads to narrow bandwidth behavior. We have $Q = \omega L/R$. With (51) and (56), the quality factor becomes

$$Q=\frac{\alpha}{\sqrt{144+2\alpha}}. \tag{59}$$

The Q factor is plotted in Fig. 9 for water-filled channels of depths between 50 μm and 400 μm. Q increases proportionally to the frequency up to a value of about 5. Beyond this point, the scaling with frequency weakens to an exponent of 1/2.

References

1. Unger M, Chou H, Thorsen T, Scherer A, Quake S. Science. 2000; 288:113. [PubMed: 10753110]
2. Grover W, Skelley A, Liu C, Lagally E, Mathies R. Sens. Actuators, B. 2003; 89:315.
3. Grover W, Muhlen M, Manalis S. Lab Chip. 2008; 8:913. [PubMed: 18497911]
4. Prakash M, Gershenfeld N. Science. 2007; 315:832. [PubMed: 17289994]
5. Pollack M, Fair R, Shenderov A. Appl. Phys. Lett. 2000; 77:1725.
6. Leslie D, Easley C, Seker E, Karlinsey J, Utz M, Begley M, Landers J. Nat. Phys. 2009; 5:231.
7. Stone H. Nat. Phys. 2009; 5:178.
8. Vedel S, Olesen L, Bruus H. J. Micromech. Microeng. 2010; 20:035026.
9. Frank O. Zeitschrift für Biologie. 1920; 71:255.
10. Frank O. Z. Biol. 1926; 85:91.
11. Morgan G, Kiely J. J. Acoust. Soc. Am. 1954; 26:323.
12. Womersley J. J. Physiology. 1955; 127:553.
13. Womersley J. Phys. Med. Biol. 1957; 2:178. [PubMed: 13484470]
14. Womersley J. Phys. Med. Biol. 1958; 2:313. [PubMed: 13567032]
15. Atabek H, Lew H. Biophys. J. 1966; 6:481. [PubMed: 19210972]
16. Hashizume Y, Phys J. J. Phys. Soc. Jpn. 1985; 54:3305.
17. Rubinow S, Keller J. J. Fluid Mech. Digital Archive. 2006; 88:181.
18. Parker K. Med. Biol. Eng. Comput. 2009; 47:111. [PubMed: 19198914]

19. Landau, LD.; Lifshitz, EM.; Kosevich, AM.; Pitaevskii, LP. Theory of Elasticity. 3rd edn. Buterworth-Heinemann; New York: 1986.
20. Seker E, Leslie DC, Haj-Hariri H, Landers JP, Begley MR. Lab Chip. 2009; 1
21. Pozar, DM. Microwave Engineering. 3rd edition. Wiley & Sons; 2005.

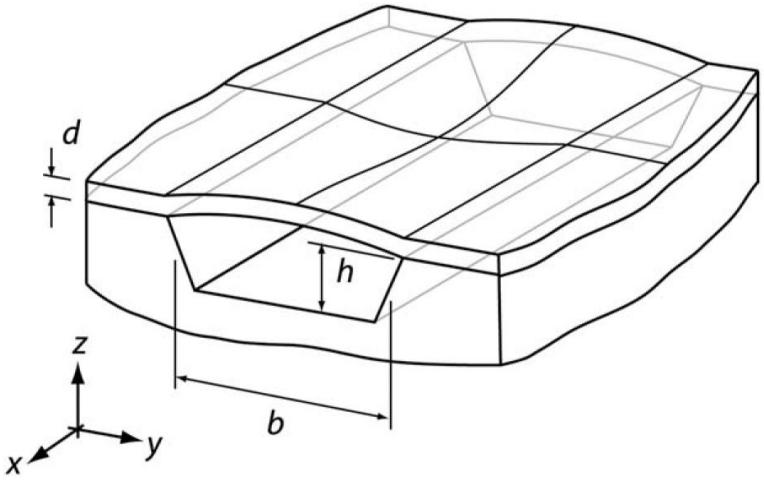

Fig. 1.
Fluidic channel etched into a rigid material, capped with an elastic cover film. *h* is the channel depth, *b* its width, and *d* is the thickness of the cover film.

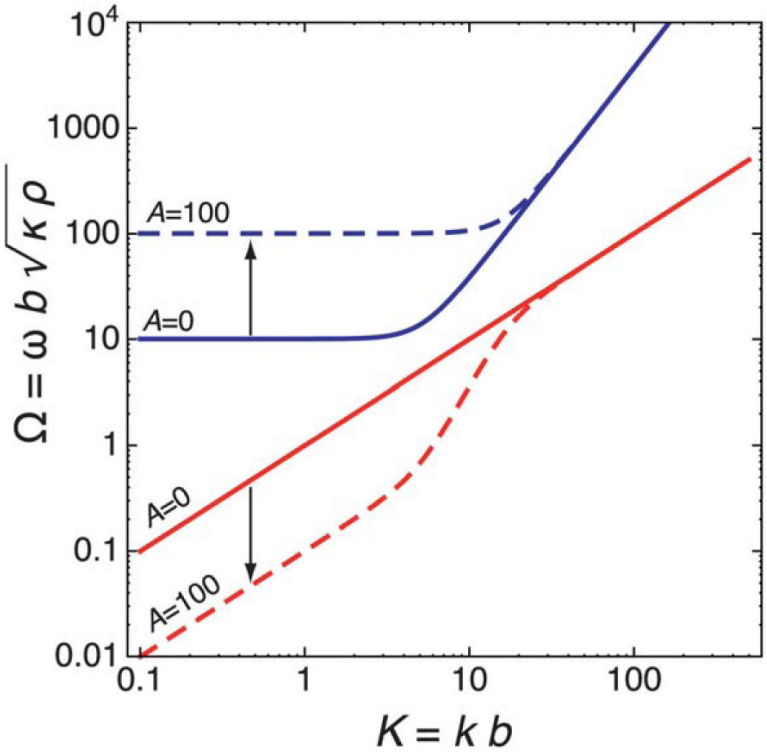

Fig. 2.
Normalized dispersion relations (solutions to (31)), calculated for $B = 10$. Solid lines: Coupling constant $A = 0$; Dashed lines: $A = 100$.

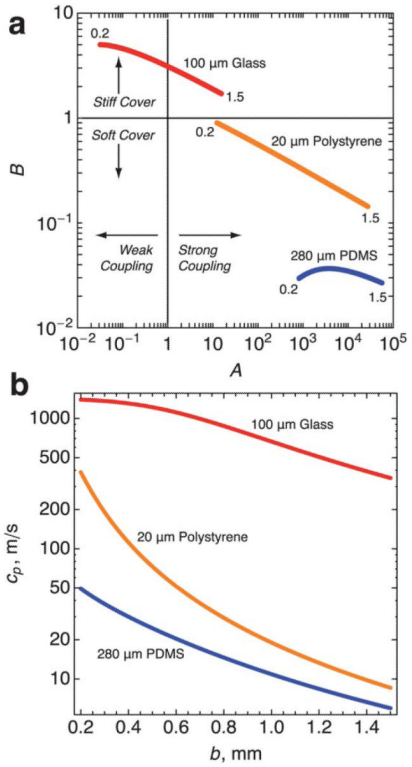

Fig. 3.

(a) Map of dimensionless parameters A and B, with values calculated for a cover made of PDMS ($\bar{E}$ =1.5 MPa; blue curve), Poly (styrene) ($\bar{E}$ =4 GPa; orange curves), and glass ($\bar{E}$ =70 GPa; red curves), for a channel depth of h = 200 μm. The channel width was varied between b = 0.2 mm and 1.5 mm. (b) Phase velocities of the small-k acoustic branch for the same cases.

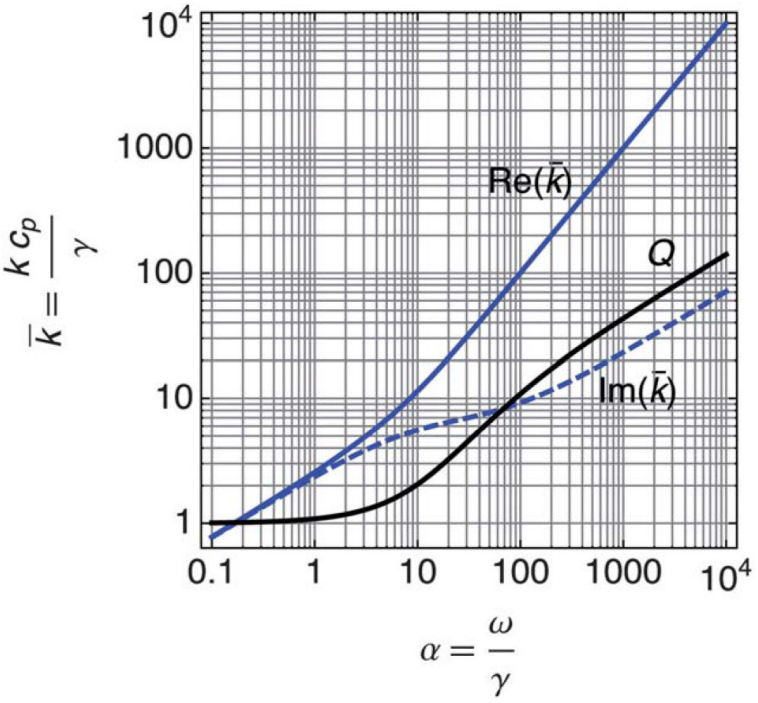

Fig. 4.

Universal dispersion relation between the non-dimensional angular frequency $\alpha = \omega/\gamma$ and the non-dimensional wave vector $\bar{k} = k_{cp}/\gamma$. The solid and dashed blue lines show the real and imaginary parts of $\bar{k}(\alpha)$; their ratio (black solid line) corresponds to the Q factor.

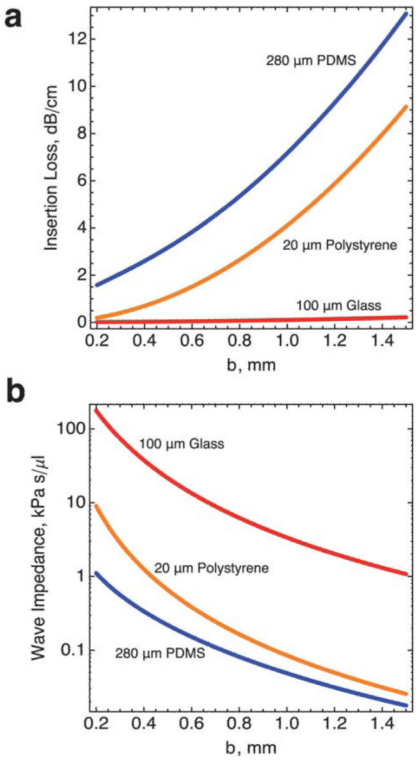

Fig. 5.

(a) Power insertion loss in dB cm^{-1} channel length at a frequency of 5 kHz for a channel of 200 μm depth, covered with either 100 μm of glass (red line), 20 μm of Poly(styrene) (orange line) or 280 μm of PDMS. (b) Wave impedance Z_0 for the same geometries.

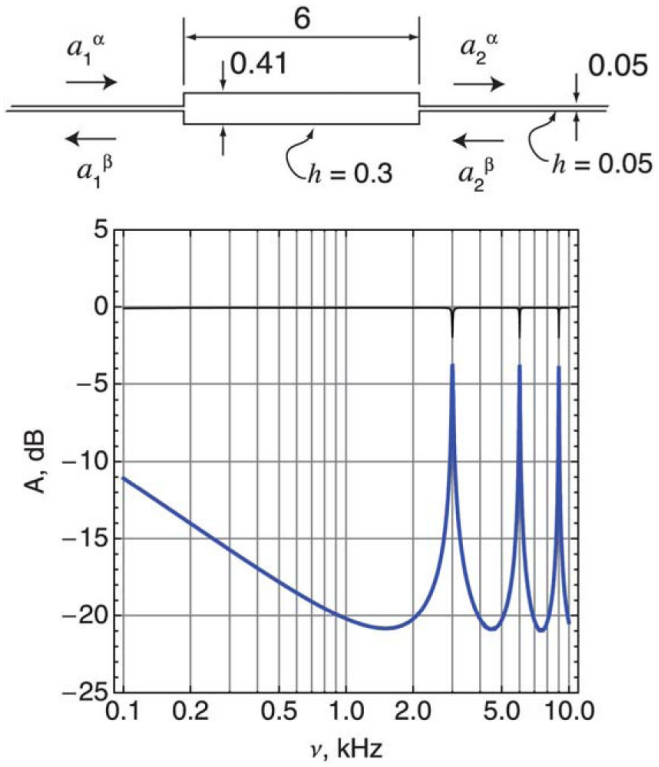

Fig. 6.

Top: Fluidic wave guide filter in series (top view, dimensions in mm). Bottom: Transmission (bold line, a_2^α/a_1^α) and reflection (thin line, a_1^β/a_1^α) ratio of the filter. Fluid properties are those of water; Cover: 280 μm PDMS.

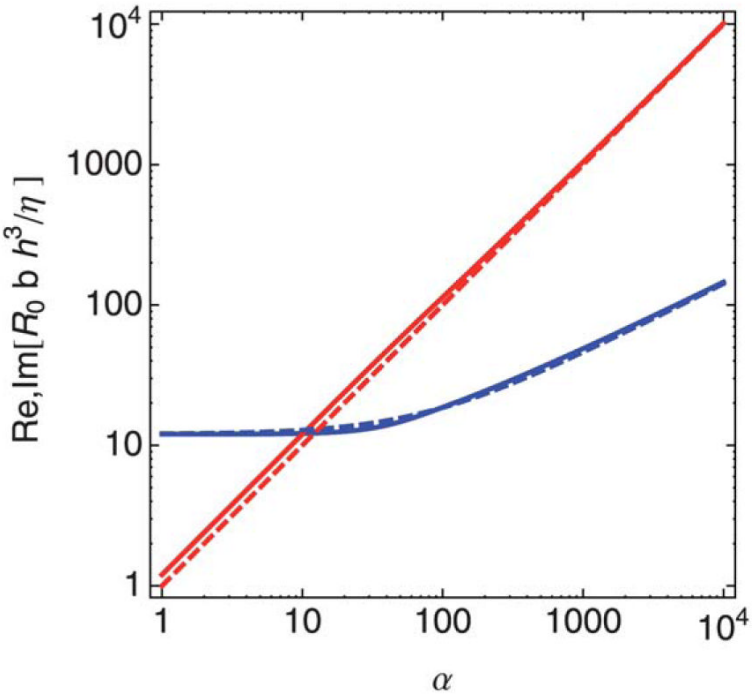

Fig. 7.

Real (red) and imaginary (blue) parts of the normalized fluidic resistance as a function of the Womersley parameter α. The solid line represents the exact solution (54), whereas the dashed lines are the approximate expression (55).

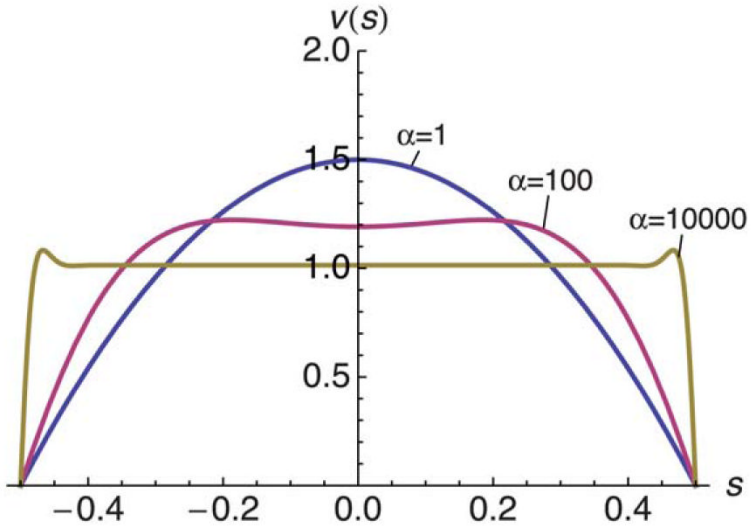

Fig. 8.
Flow profiles Re[$v(s)$] computed from (50) for values of $\alpha = 1$, $\alpha = 100$, and $\alpha = 10\,000$.

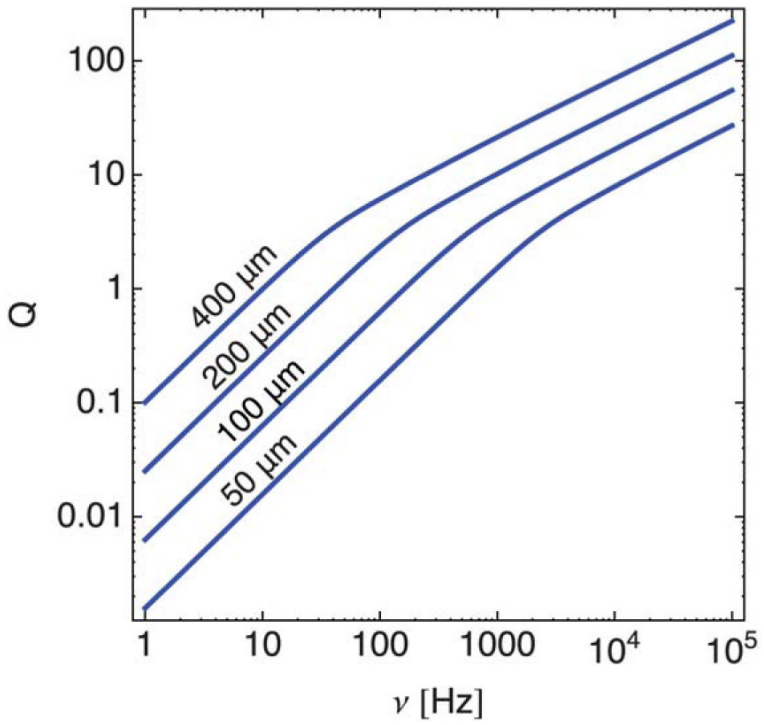

Fig. 9.
Channel quality factor Q as a function of frequency for water filled channels of 50, 100, 200, and 400 μm depth.